JOURNAL OF GEOPHYSICAL RESEARCH, VOL. 105, NO. D19, PAGES 24,375–24,386, OCTOBER 16, 2000

A convective kinematic trajectory technique for low-resolution atmospheric models

S. R. Freitas,[1] M. A. F. Silva Dias, and P. L. Silva Dias

Departamento de Ciências Atmosféricas, University of São Paulo, São Paulo, Brazil

K. M. Longo[1] and P. Artaxo

Instituto de Física, University of São Paulo, São Paulo, Brazil

M. O. Andreae and H. Fischer

Max Planck Institute for Chemistry, Mainz, Germany

Abstract. This paper presents a simple methodology to take into account the subgrid effects of wet convective processes to trace vertical motion of air parcels for low-resolution atmospheric models. Such models are used for wind field simulations that serve as input for trajectory models. Air parcels in moist convective regions can thus be vertically transported to the cumulus top level with the short timescale associated with cumulus updrafts. Two cases are presented: wet and dry seasons in Amazonia, showing the differences of trajectories followed by air parcels with and without the methodology. The implications for the interpretation of air chemistry measurements are discussed, and an example using LBA/CLAIRE data is used to point out the usefulness of the convective kinematic trajectory technique presented here.

1. Introduction

Air parcel trajectories have been used extensively in atmospheric chemistry studies on the transport of gases and particulate matter emitted by biomass burning and other pollution sources. The transport of these atmospheric pollutants, either in a regional or in a long-range perspective, depends primarily on the atmospheric structure of turbulence in the planetary boundary layer and on the wind field, which will disperse and advect the air mass, respectively. The occurrence of deep cumuli near polluted regions may play an important role in the transport process, since they can carry the pollutants to the upper troposphere, where the winds are faster and the residence times can be longer. *Dickerson et al.* [1987] showed a direct observation of convective transport of trace gases by deep cumuli next to the Oklahoma-Arkansas border (United States). *Pickering et al.* [1996a] described an observation of deep convective transport of trace gases by a series of large mesoscale convective systems that occurred over Brazil during the Transport and Atmospheric Chemistry Near the Equator - Atlantic (TRACE-A) experiment [*Fishman et al.*, 1996]. *Thompson et al.* [1994] have discussed the importance of this transport mechanism for CO and other precursors in tropospheric ozone formation.

Several authors have been working with air parcel trajectory calculations in backward and forward modes. Back trajectories are typically used for the interpretation of chemical measurements, and forward trajectories are used in atmospheric research flight planning and in Lagrangian modeling. As spatial and temporal resolution of meteorological observations limit the accuracy of trajectory calculations, several techniques have been employed to provide verification of trajectory models [*Kuo et al.*, 1985; *Kahl et al.*, 1986; *Haagenson et al.*, 1987].

Because of the extreme scarcity of observations, several studies on air pollution transport over the Southern Hemisphere have used the analyzed gridded data sets generated by the major operational weather analysis and forecast centers for computing trajectories. *Pickering et al.* [1994] compared isentropic trajectories computed from meteorological fields in the analyses of the National Center for Environmental Prediction (NCEP) and of the European Centre for Medium-Range Weather Forecasts (ECMWF). Their results indicate large differences between the trajectories based on the two fields in terms of travel distance, horizontal separation, and vertical separation. *Pickering et al.* [1996b]

[1]Now at NASA Ames Research Center, Moffett Field, California.

Paper number 2000JD900217.
0148-0227/00/2000JD900217$09.00

used meteorological observations obtained from the TRACE-A experiment for intercomparison of trajectories computed from NCEP and ECMWF meteorological analyses and showed that the ECMWF analyses are slightly better at reproducing observed conditions than the NCEP analyses in the tropics and subtropics of the Southern Hemisphere. However, both analyses differ from the observed soundings to a significant degree, and the resulting trajectories indicate large differences.

Additional uncertainty results from the choice of the technique for calculating trajectories. Isentropic trajectories have been used widely [e.g., *Pickering et al.*, 1994, 1996] and have the advantage that they do not require the vertical wind velocity. The kinematic approach uses the three components of wind velocity for trajectory calculation and does not make explicit assumptions about the air parcel motion. However, the vertical velocity data needed are subject to considerable uncertainty. *Fuelberg et al.* [1996] computed kinematic and isentropic trajectories during a single 5-day period of the TRACE-A experiment using ECMWF analyses. Their results showed that kinematic trajectories usually indicated considerably greater vertical displacements and are more accurate than their isentropic counterparts. However, both approaches may yield realistic 5-day trajectories.

With the advance of computational power and the use of mesoscale atmospheric models, one may calculate more realistic trajectories from atmospheric simulations with an observational data assimilation system, better spatial and temporal resolution and more complete physics [*Freitas et al.*, 1996; *Longo et al.*, 1999]. The improved model spatial resolution in this case is defined by the available computational capability. For long-range transport studies, usually the computational limitations impose the use of models with spatial resolution that is not enough to resolve explicitly convective processes such as deep convection. Erroneous trajectories can result if the role of deep convection at the resolved scale is not included adequately. Since deep convection produces strong ventilation from the boundary layer to upper levels, its neglect can have severe consequences for the predicted transport of atmospheric pollutants.

This study presents a simple methodology that accounts for subgrid scale moist convective processes in the air parcel vertical velocity for low-resolution atmospheric models. The air parcels in moist convective regions can be vertically transported to the cumulus top at the short timescale associated with cumulus updrafts. This method is based on the University of São Paulo Trajectory Model [*Freitas et al.*, 1996; *Longo et al.*, 1999], a sigma-z kinematic three-dimensional model coupled to the Regional Atmospheric Modeling System (RAMS) [*Tripoli and Cotton*, 1982; *Pielke et al.*, 1992].

2. Convective Trajectory Technique

Atmospheric motion is governed by nonlinear equations that represent a broad range of spatial scales. It is necessary to distinguish between those eddies that can be numerically resolved and the remaining eddies that are not fully resolved by the numerical solutions. The eddies associated with cumulus convection are not explicitly resolved in large-scale atmospheric models. Nevertheless, it is well known that cumulus convection can have an important effect on the dynamics and energetics of larger-scale motion. Cumulus parameterization is generally used in large-scale atmospheric models to take into account the convective heat, moisture, and momentum transport by cumulus convection [see *Emanuel and Raymond*, 1993, for a review]. In analogy to the parameterization of cumulus convection the air parcel kinematic trajectory calculation should account for the effects of cumulus convection on the vertical velocity $\overline{w}$ in the equation

$$\overrightarrow{r}(t) = \overrightarrow{r}(t_0) + \int_{t_0}^{t} (\overline{u}, \overline{v}, \overline{w}) dt, \tag{1}$$

where $\overrightarrow{r}(t)$ is the air parcel position in space at time t and $(\overline{u}, \overline{v}, \overline{w})$ are the three components of wind of the large-scale model. In this way, an air parcel reaching a moist convective region could be vertically transported to cloud top.

The subgrid effect of cumulus convection parameterization on the large-scale vertical velocity can be obtained from the "top-hat " method [*Anthes*, 1977]. In equations (2) through (8) we will review the basic description of this sub-grid parameterization. In the top-hat model, the clouds are assumed to be described by characteristic values of the dynamic and thermodynamic variables, while the cloud-free environment has its own characteristic values. The fraction of the horizontal area of a grid cell covered by cumulus clouds is designated by a, and $(1 - a)$ is the fraction occupied by the cloud-free environment. In this framework the average of the vertical velocity in the grid cell can be obtained by

$$\begin{aligned} \overline{w} &= \frac{1}{\Delta x \Delta y} \int_{x-\frac{1}{2}\Delta x}^{x+\frac{1}{2}\Delta x} \int_{y-\frac{1}{2}\Delta y}^{y+\frac{1}{2}\Delta y} w dx dy \\ &= a\overline{w_c}^c + (1-a)\overline{w_e}^e, \end{aligned} \tag{2}$$

where the operators $\overline{(\,)}^c$ and $\overline{(\,)}^e$ denote horizontal averages over the cloud and cloud-free regions, respectively. The parameter a is fixed at 2% in accordance with previous estimates by *Malkus et al.* [1961] and *Anthes* [1977].

Hereafter, cloud downdrafts will be ignored and only updraft velocity will be considered as the mean cloud velocity in the large-scale equations, following the discussion of *Anthes* [1977]. The non inclusion of convective downdrafts will imply that midtropospheric air parcels when encountering a convective grid point will have as an only option the ascent to upper levels. Clearly, some portion of these midtropospheric parcels might be transported downward and affect the low-level concentrations. However, for the boundary layer parcels, the main effect is the ascent in updrafts. Since

in this first attempt the interest is on the long-range transport of boundary layer accumulated constituents, the trajectories will be presented for air parcels initiated in the boundary layer or in upper levels thus minimizing the impact of the neglect of convective downdrafts. The inclusion of the downdrafts is still in test and will be included in future versions of the model.

The vertical velocity of the cumulus clouds is obtained from *Simpson and Wiggert* [1969]:

$$\frac{1}{2}\frac{dw_c^2}{dz} = \frac{gB}{1+\alpha} - gQ_{lw} - \mu w_c^2, \tag{3}$$

where w_c is the vertical velocity of the updraft, g is gravity, μ is the entrainment rate in the cumulus updraft, α is the "virtual mass coefficient" (0.5), which compensates for the neglect of nonhydrostatic pressure perturbations, and Q_{lw} is the total liquid water mixture ratio. The buoyancy term B is given by

$$B = \frac{T_v - T_{ve}}{T_{ve}}, \tag{4}$$

where T_v and T_{ve} are the virtual temperatures of the updraft and the environment. The entrainment rate is given by

$$\mu = \frac{0.183}{R}, \tag{5}$$

where R is the radius (m) of the updraft, and R=5000 m has been used in this study corresponding to 2 - 3% of the grid area. To estimate the liquid water Q_{lw} in the air parcel updraft, the following simplification has been assumed:

$$Q_{lw} = -c\Delta r_s = -c(r_s - r_s^{\mathrm{LCL}}), \tag{6}$$

where r_s is the saturation mixing ratio of updraft, and c is a constant determined by an iterative process, so the vertical velocity of the updraft is less than 1 cms^{-1} at cloud top. Once the cloud thermodynamic model, described below, supplies the lifting condensation level (LCL) and cloud top level (TOPCL), equation (3) is integrated with the boundary condition

$$w_{c,\mathrm{LCL}} = \max(1\ \mathrm{m/s}, w^*), \tag{7}$$

where w^* is the vertical velocity at the LCL of an air parcel updraft, due to the turbulent process in the subcloud layer, given by [*Albrecht et al.*, 1986]

$$w^* = \left[gZ_{\mathrm{LCL}} \frac{\left(\overline{w'T_v'}\right)_0}{T_0} \right]^{1/3}, \tag{8}$$

where Z_{LCL} is the LCL height, $\left(\overline{w'T_v'}\right)_0$ is proportional to the sensible heat flux at the surface, and T_0 is the surface air temperature; the lower value of 1 m/s is obtained of *Anthes* [1977].

The vertical transport by deep convection has been implemented in the RAMS version 3b. Deep convection in RAMS is parameterized through a Kuo-type scheme modified by *Molinari* [1985] and *Tremback* [1990]. The one-dimensional cloud model used in the cumulus parameterization of RAMS uses a parcel sounding computed by the appropriate moist adiabatic equations modified by entrainment given by equation (5):

$$\frac{\partial \theta_E}{\partial z} = \mu\left(\theta_E^e - \theta_E\right), \tag{9}$$

where θ_E^e is the environment equivalent potential temperature.

The cumulus parameterization of RAMS 3b requires the following steps: 1) convection is activated if the grid column is convectively unstable and if there is a resolved upward vertical motion above a specified threshold at the LCL; 2) the air source level for convection is defined at the highest θ_E below a 3 km height. The LCL of the source level air is determined; 3) cloud top is defined as the level where the potential temperature of the moist adiabat modified by entrainment becomes less than the grid point potential temperature; 4) the vertical profiles of heating and moistening are computed; 5) the convective tendency terms for potential temperature, and total water are determined.

The convective heating term, given by the cumulus parameterization, enhances the vertical motion at the resolved scale $\overline{w}$. However, as will be shown below, this is not sufficient for the calculation of 3-D kinematic trajectories under highly convective conditions. The method proposed in this paper reinforces the cumulus convection effects in the vertical velocity field obtained by the atmospheric model so that air parcels in convective regions can be vertically transported to the cumulus top at the short timescale associated with cumulus updrafts. This goal can be achieved assuming that the vertical velocity for trajectory calculations is given by an area-weighted average between the environment vertical velocity and the convective velocity, in the following way:

$$\overline{w}_{\mathrm{conv\_traj}} = (1-a)\overline{w} + aw_c, \tag{10}$$

where $\overline{w}$ is the large-scale vertical velocity given by the atmospheric model and $\overline{w}_{\mathrm{conv\_traj}}$ is the vertical velocity used by the trajectory model. Thus the convective kinematic trajectory calculation is obtained by the equation

$$\overrightarrow{r}(t) = \overrightarrow{r}(t_0) + \int_{t_0}^{t} (\overline{u}, \overline{v}, \overline{w}_{\mathrm{conv\_traj}})dt. \tag{11}$$

The University of São Paulo Trajectory Model (USPTM) [*Freitas et al.*, 1996; *Longo et al.*, 1999] is a sigma-z kinematic three-dimensional model coupled to the RAMS 3b model, which uses the three components of the wind for determination of air parcel trajectories. Forward or backward trajectories can be computed using the nesting capability of RAMS. The method to solve equation (1) is described by *Petterssen* [1956]. *Seibert* [1993] discusses the numerical aspects of this scheme and shows that the numerical solution is accu-

rate to the second order. During the RAMS simulation the wind fields and convective information generated are stored for later use in USPTM.

Once the wind fields and convective information are stored, the model can generate the trajectories in the nonconvective mode, when only the resolved winds are used, or in convective mode, when equation (10) is used to include the subgrid convective process.

3. Uncertainties in the Technique

The main uncertainties of the proposed technique are the following: (1) the weighted average defined in equation (10), (2) the fractional area covered by updrafts a, and (3) the convective parameterization parameters (LCL, cloud top level, convective available potential energy (CAPE)) and the location and duration of simulated cloudiness.

The most critical aspect of the technique is related to the location and duration of the simulated clouds given by the convective parameterization as well as the large-scale conditions. A wrongly located, in space or time, simulated convective cloud will provide inadequate description of the trace gas transport and meaningless trajectories. Therefore the simulated cloud location and duration should be the first aspect in a validation process.

Given an adequate modeling of clouds, the next debatable item is the vertical velocity used in the convective trajectories. Equation (10) defines an areal-weighted average between resolved scale vertical velocity and cloud scale vertical velocity following the top-hat philosophy. Other definitions could be given, as the one suggested by an anonymous reviewer whereby a parcel would be transported by resolved scale velocity or cloud scale velocity generating two sets of trajectories associated to given probabilities based on the fractional cloud cover a. This alternative method will be introduced in future versions and compared with the top-hat approach. However, it should be noted that the vertical velocity used in the trajectory computation

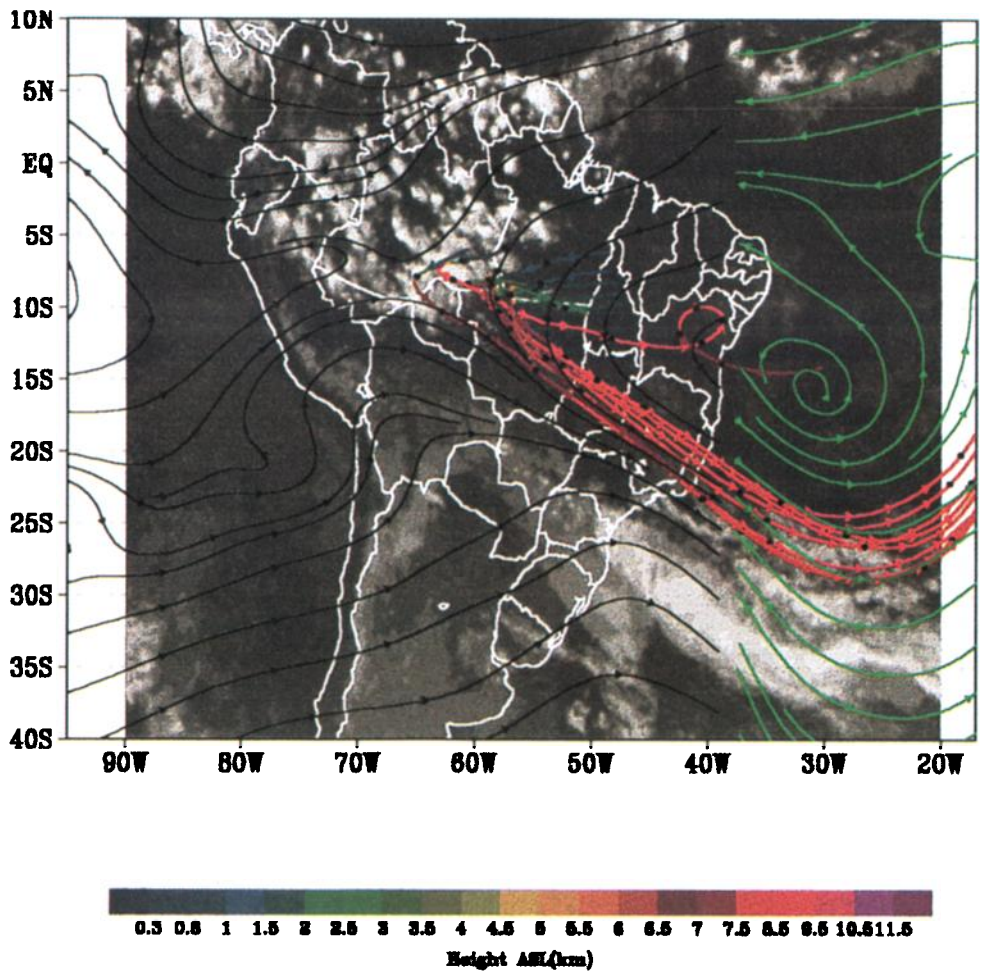

Plate 1. Forward trajectories, calculated in the convective mode, initialized at 0000 UTC on July, 11, 1993, and at 1000 m above the ground level (agl). IR satellite image at 0000 UTC, July 13, showing convective activity over the Amazon Basin. Streamlines in black are for 0000 UTC, July 13, and at 7500 m agl. Streamlines in green are for 0000 UTC July 16, and at 8500 m agl. The color scale represents the height above sea level of air parcel in kilometers and each dot on the trajectory represents a 24 hour interval.

will affect mainly the time interval for a parcel to reach cloud top. The cloud top is given by the grid point thermodynamic profile and parcel initial conditions, thus the level of detrainment is basically independent of the vertical velocity used, under the conditions observed in this study. The large-scale horizontal wind evolution at the detrainment level may provide some uncertainty in the trajectory computation at that level.

Finally, the fractional area covered by updrafts has been fixed in 2%. *Anthes* [1977] uses a relationship based on the ratio between grid scale and cloud scale precipitation. For the present case, the ratio suggested by Anthes gave values of $a < 0.5\%$, which we considered too low based on values listed in the literature [*Malkus et al.*, 1961; *Anthes*, 1977]. A value of a, which is excessively low, may affect the level of detrainment since horizontal advection would remove the parcel from the updraft area before reaching cloud top. A compromise in this work has been to fix a with a value that has been suggested in the literature. Other possibilities could be an estimate of updraft area obtained by satellite. However, most of the available products give the fractional area covered by clouds or the mean convective cloud cover which would represent an overestimate of updraft area. Further tests with remotely sensed products will be introduced in the future.

4. Case Studies

4.1. Dry Season

The dry season in central Brazil and the Amazon region lasts from June to October and is characterized by intense biomass burning [*Crutzen and Andreae*, 1990]. Large emissions of trace gases and aerosol particles have been detected and reported by several authors [*Andreae et al.*, 1988; *Artaxo et al.*, 1994, 1998]. These studies discuss the local and regional impacts and the possibility of long-range transport of pollutants, which could have a continental or even hemispheric impact [*Chatfield and Delany*, 1990; *Chatfield et al.*, 1996].

From the climatological point of view, central Brazil is dominated from June to September by a high-pressure area with little precipitation and light winds at lower levels [*Satyamurti et al.*, 1998]. However, on a day-by-day basis the transient phenomena associated with midlatitude weather systems, equatorial waves, and local circulation represent perturbations that may lead

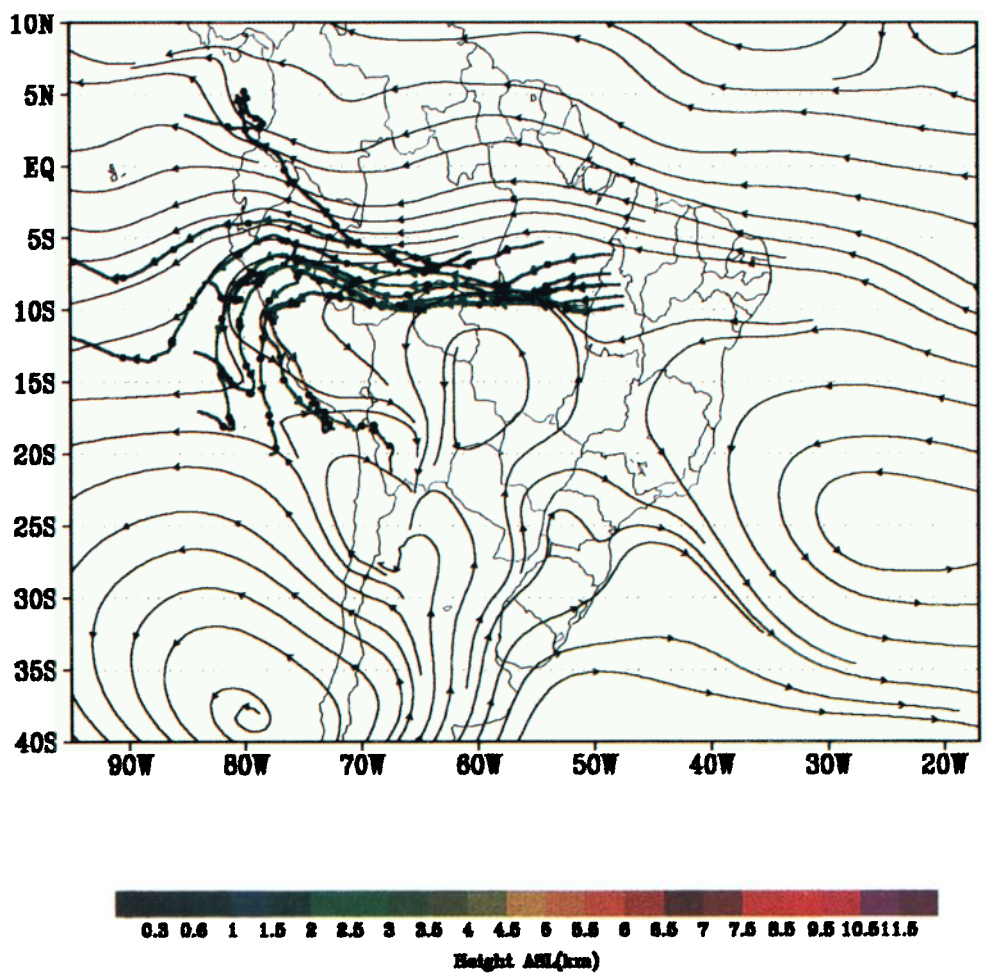

Plate 2. Same trajectories as in Plate 1 but calculated in the nonconvective mode. Streamlines are for 0000 UTC, July 13 and at 1500 m agl.

to a quite different picture. The approach of midlatitude fronts from the south, as reported by *Kousky and Ferreira* [1981] and *Fortune and Kousky* [1983], changes the atmospheric stability and the wind field. The propagating squall lines originating along the northern coast of Brazil [*Silva Dias and Ferreira*, 1992; *Cohen et al.*, 1995] present another type of convective perturbation typical of the dry season.

The period from July 11 to 20, 1993, will be discussed as a case study in this section. The RAMS simulations were performed on 200 km grid resolution covering South America, most of Central America, and neighboring oceans. A nested grid with a 50 km resolution was located over South America. For the coarse grid the vertical resolution starts at 450 m at the lowest level, stretching at a rate of 1.2 to a vertical resolution of 1100 m, which was then kept constant up to the model top located at approximately 20 km. The number of layers was 23. The nested grid vertical resolution began at 150 m increasing up to 1100 m by a factor of 1.2, with the model top at approximately 16 km. The number of layers was 29. The physical parameterizations included were the anisotropic turbulence dependent on the deformation tensor, atmospheric long and short wave radiation interacting with water vapor and liquid water, surface interaction, including a vegetation and a soil model, and the parameterized effect of deep cumulus clouds. The initial conditions were obtained from the US National Center for Environmental Prediction (NCEP) - 2.5° reanalysis [*Kalnay et al.*,

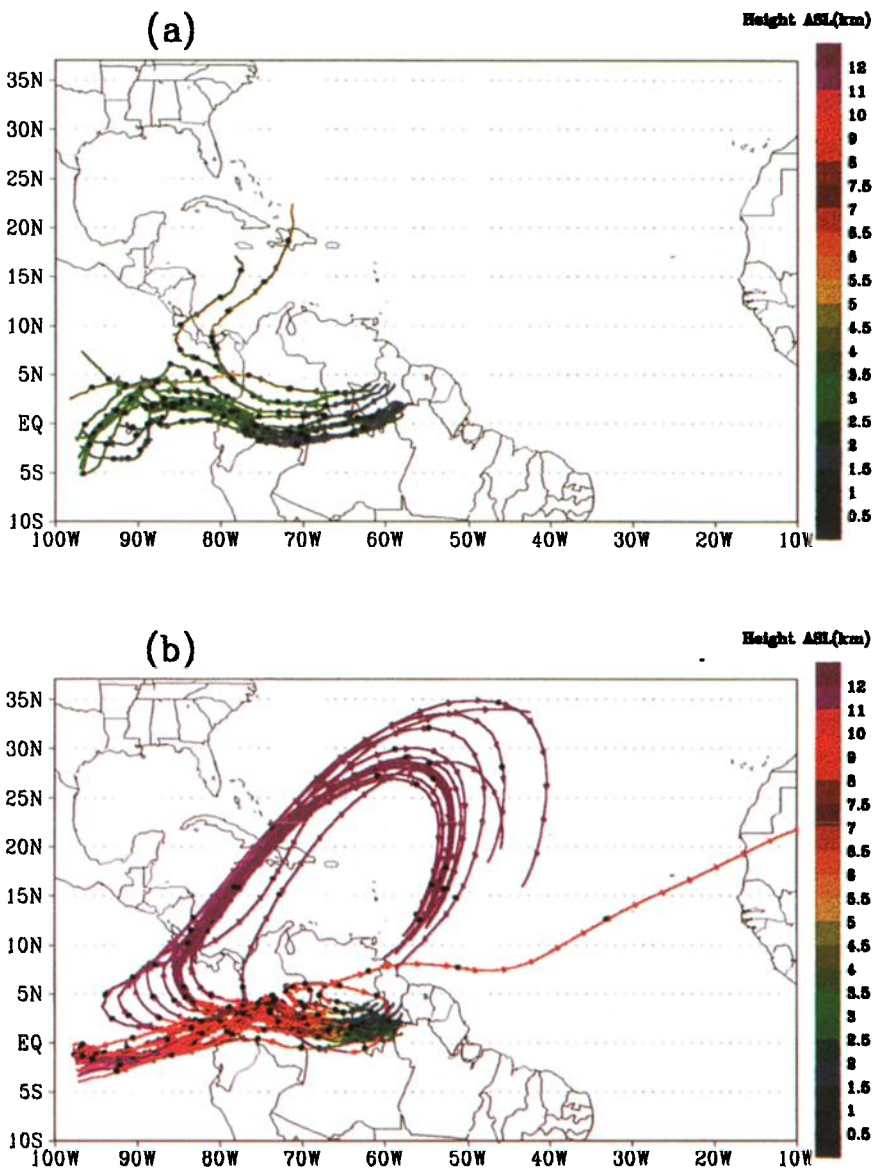

Plate 3. Forward trajectories calculated in the nonconvective mode (a) and in the convective mode (b), starting at 2000 UTC, March 16, and at 1500 - 2000 m agl over Roraima. The color scale represents the height above sea level of air parcel in kilometers, and each dot on the trajectory represents a 24 hour interval.

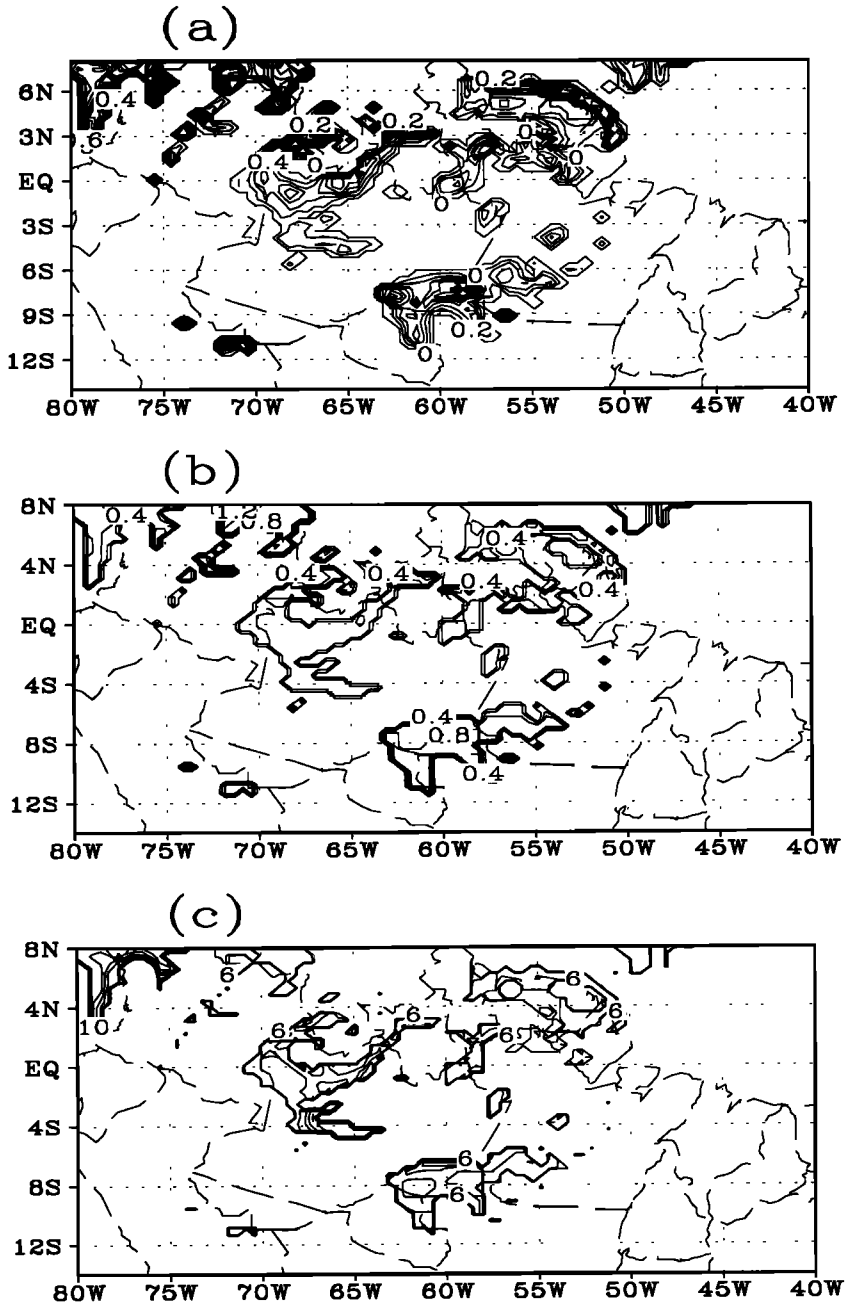

Figure 1. (a) Convective precipitation rate (mm h^{-1}), (b) lifting condensation level height (km agl) and (c) cloud top height (km agl) simulated by RAMS at 0000 UTC, July 13, 1993.

1996]. The model was nudged at every time step toward the NCEP reanalysis, available every 6 hours, at the boundaries and model top and, to a lesser extent, at the model center. The wind fields and convective information were stored every 2 hours of simulation as the input to the trajectory model. The time step for the trajectory calculation was of 10 min.

The example to be discussed refers to a cluster of trajectories initialized at 0000 UTC on July 11, 1993, over central and northern Brazil, and at 1000 m above the ground level. Plates 1 and 2 show the trajectories calculated in the convective and nonconvective modes, respectively. Plate 1 shows the trajectories, wind fields, and the infrared satellite image at 0000 UTC on July 13. These trajectories were calculated using the output from the coarse and nested grids. The integration began in the nested grid and follows the air parcels until they reach the boundary. Then, the coarse grid output is used to complete the trajectories. The color scale represents the height above sea level of the air parcel in kilometers, and each dot on the trajectory represents a 24 hour interval. During the first 48 hours the air parcels were transported to the west and southwest by the low-level circulation, reaching a moist convective re-

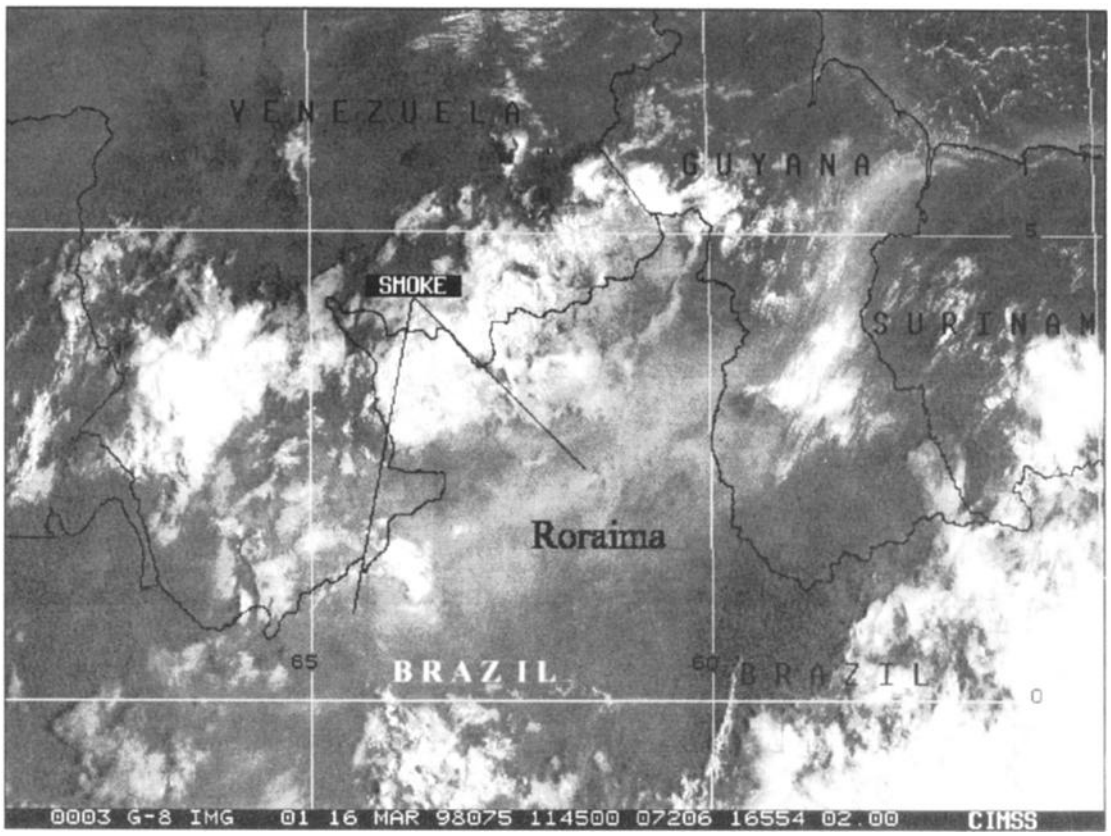

Figure 2. GOES-8 visible satellite image at 1145 UTC, March 16, 1998, showing the smoke produced by biomass burning over the Brazilian State of Roraima.

gion at 0000 UTC on July 13. Figure 1a shows the convective precipitation rate (mm/h) at 0000 UTC on July 13, while Figures 1b and 1c show the LCL and TOPCL heights, respectively. The LCL was located around 800-1000 m and the TOPCL at about 6000-8000 m above the surface.

The convective trajectories (Plate 1) were associated with an enhanced upward vertical motion up to the top of the convective system. The duration of this transport was about 6 - 8 hours, with a vertical velocity of approximately 20 cm/s. At the scale of the cloud this speed represented an average updraft w_c of 10 m/s. During this period the largest value of the large-scale vertical velocity $\overline{w}$ was of the order of 2 cm/s, staying, however, generally smaller than 1 cm/s. After the convective period the air parcels stayed around this level (8000 m), being advected to the southeast by the horizontal wind, following the airflow indicated (streamlines in black, corresponding to 0000 UTC, July 13, and at 7500 m above surface level). The cluster of trajectories more to the south stayed for 4 days inside the nested grid domain, while the northernmost trajectories (in red) stayed for 9 days before reaching the boundary. When these trajectories reached the inner grid boundary, they were at about 8000-9000 m above sea level. It takes about 30 hours more to reach the coarse grid boundary, following an anticyclonic flow over the Atlantic Ocean (streamlines in green, corresponding to 8500 m above surface level and at 0000 UTC July 16, 24 hours after crossing the nested grid boundary). The air parcels traveled about 20° of longitude with an average horizontal speed above 70 km h^{-1} and at a height level between 7500 and 9000 m above sea level.

Plate 2 indicates that air parcels in the nonconvective trajectory simulation were being vertically transported at a resolved vertical velocity $\overline{w}$ of at most 2 cm/s, and therefore the horizontal advection dominated the transport. Consequently, the air parcel is removed from the convective area in a time period that is not enough for reaching the top of the cumulus. The nonconvective trajectories followed the trade wind circulation at low levels shown in Plate 2 (streamlines corresponding to 0000 UTC, July 13, and at 1500 m above surface level), traveling at opposite direction and lower height levels than their convective counterparts shown in Plate 1. The configuration of the wind field at levels from 2000 to 3000 m (not shown) was very similar to the one shown in Plate 2, in agreement with the paths of the nonconvective trajectories shown. The trajectories that cross the Andes Mountains around 5°S take about 5.5 days to reach the nested grid boundary.

4.2. Wet Season

The case studied during the wet season refers to the month of March 1998, when intense biomass burning over the northwest of the Amazon Basin was observed

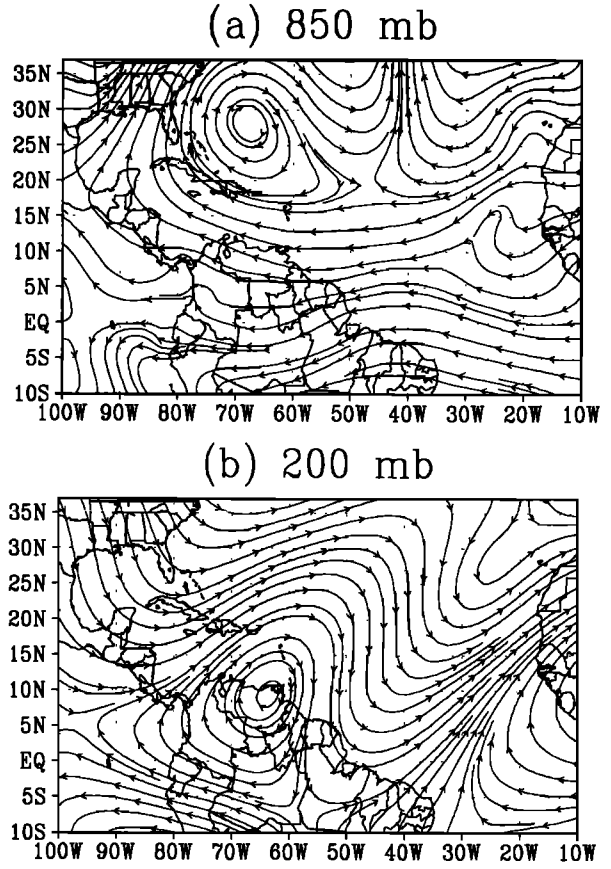

Figure 3. (a) Time average over the first three days (0000 UTC, March 16, to 0000 UTC, March, 19, 1998) of the wind field at 850 mbar height and (b) time average over the last three days (0000 UTC, March 23, to 0000 UTC, March 26, 1998) of the wind field at 200 mbar height.

(mainly over the Brazilian state of Roraima). This particular month was hotter and drier than the climatological average, due the activity of the "El Niño" atmospheric phenomenon [*INPE*, 1998]. The northern Amazon Basin was under strong subsidence, which lead to low precipitation. Figure 2 shows the GOES-8 visible satellite image at 1145 UTC, March 16, 1998, when smoke produced by biomass burning over Roraima is advected to the southwest. During this period the atmospheric chemistry experiment LBA-CLAIRE (Cooperative LBA Airborne Regional Experiment) took place and observations of gases and aerosol were obtained with instrumented aircraft.

To study the atmospheric transport of the biomass burning emissions, the output from the RAMS simulation was stored every 2 hours. The simulation started at 0000 UTC, March 15, 1998, and carried on for 30 days, using the NCEP 2.5° reanalysis, to supply the initial and boundary conditions. In the first 15 days of simulation the wind field configuration presented two important characteristics: at low levels, strong onshore (NE) flow onto the NE coast of the Guyanas and Brazil, shown in Figure 3a as the time average in the first three days of the wind field at 850 mbar height corresponding to the beginning of the trajectories, and at higher levels an anticyclonic flow over the northern part of South America as shown in Figure 3b, as the time average in the last three days of the wind field at 200 mbar height corresponding to the last part of the trajectory calculations.

Air parcel forward trajectories were calculated for 10 days, starting at 2000 UTC, March 16, and at 1500 m above surface level over Roraima. Plates 3a and 3b show the trajectories calculated in the nonconvective mode and convective mode, respectively. Initially, during first 1-2 days, both clusters of trajectories follow the northeast flow, indicating the air parcels being advected to the southwest at low levels. However, deep convective systems over the northwestern Amazon impose strong upward motion to the air parcels. The cluster of convective trajectories (Plate 3b) shows the air parcels being vertically transported to the cloud top level (at approximately 8 km), in a time period of a few hours. The GOES-8 IR satellite image at 1800 UTC, March 18 (Figure 4), shows the convective system responsible for the upward transport that was adequately represented in the RAMS simulation. At higher levels, some air parcels continue to be transported to the west, while others follow the anticyclonic flow over the Atlantic Ocean coming back to the South American continent. All the nonconvective trajectories (Plate 3a) continue to the west at lower levels.

During Flight 8 of the LBA-CLAIRE experiment, over Suriname on March 26, 1998, the aircraft detected at high altitudes (>9 km) an air mass with a chemical composition characteristic of aged biomass burning smoke [M. O. Andreae et al., Transport of biomass burning smoke to the upper troposphere by deep convection in the equatorial region, submitted to *Nature*, 2000]. Figure 5 shows the vertical profile of carbon monoxide and carbon dioxide concentrations measured at this flight. A layer enriched in pyrogenic trace gases (CO, CO_2, various hydrocarbons, acetonitrile, and methyl chloride) and aerosols was observed at about 10 km, located over a clean air column. The trace gas and aerosol enrichments were highly correlated, and the correlation slopes had values characteristic of highly aged smoke. Ozone was also enriched, indicating photochemical ozone production in the plume. The trajectories calculated in the convective mode (Plate 3b) show the atmospheric transport mechanisms responsible for the transfer of biomass burning pollution from the boundary layer to the upper troposphere: (1) transport from the fires in the Roraima region to the western convective areas, (2) lifting of the smoke-laden air to the upper level by deep convection systems, and (3) transport around a high-altitude anticyclone to the Guyana/Suriname region. The trajectories obtained in the nonconvective mode (Plate 3a), on the other hand, cannot explain the LBA-CLAIRE aircraft observations.

5. Summary and Conclusions

We have described a simple methodology that takes into account the subgrid scale moist convective processes

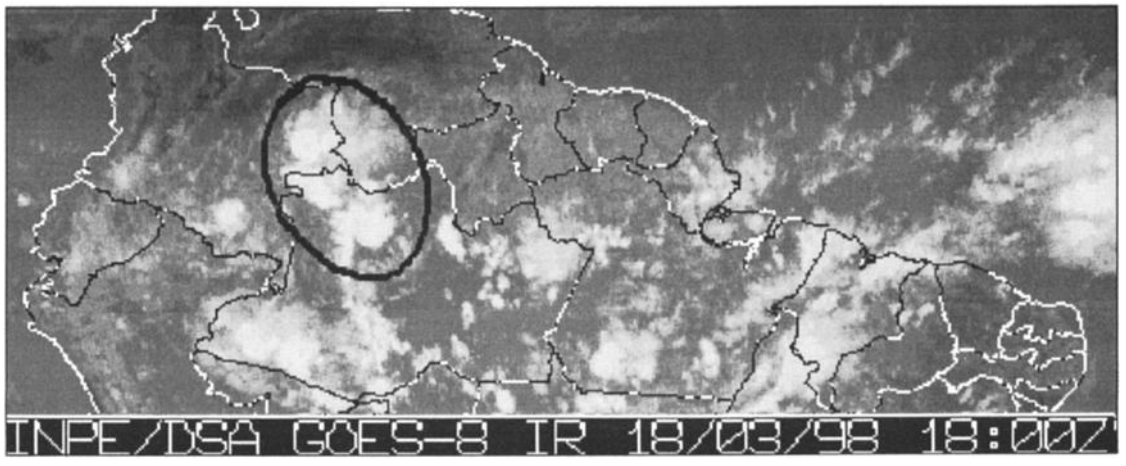

Figure 4. GOES-8 IR satellite image at 1800 UTC, March 18, 1998 showing the convective systems in the northern part of the Amazon Basin.

in the air parcel vertical velocity for low-resolution atmospheric models. These models are being used for wind field simulations that serve as input for trajectory models. With this methodology, air parcels in moist convective regions can be vertically transported to the cumulus top at the short timescale associated with cumulus updrafts. The technique was applied to two case studies in the dry and wet seasons in Amazonia during

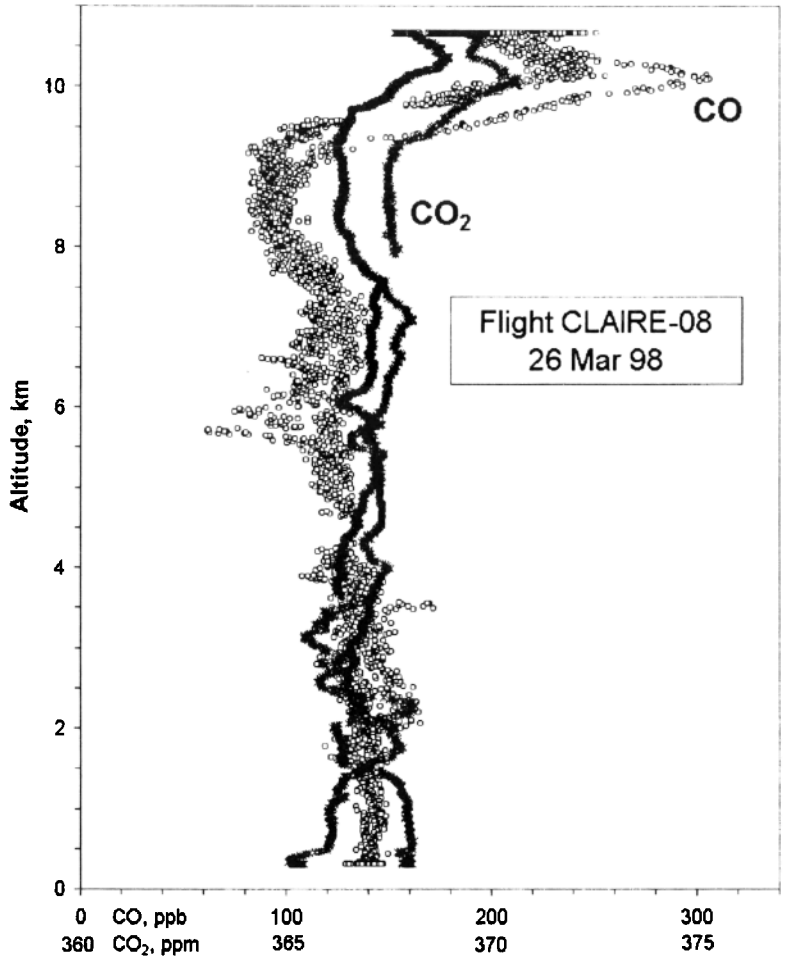

Figure 5. Vertical profiles of carbon monoxide (ppb) and carbon dioxide (ppm) observed during flight number 8 (March 26, 1998) over Suriname and Guyana.

events of biomass burning. In both cases the trajectories calculated in the convective and nonconvective modes show large differences leading to very different interpretations.

For the wet season case, experimental evidence during the LBA-CLAIRE campaign indicates that the trajectories calculated in the convective mode present a better picture of the deep convection process than the traditional approach. The transport description simulated was fully consistent with observations (satellite images and aircraft observations of biomass burning plumes in the upper troposphere), depicting the main processes responsible for the transfer of biomass burning emissions from the planetary boundary layer to the upper troposphere.

Acknowledgments. This work was sponsored by the Brazilian agencies FAPESP, CNPq and CAPES-PICD. LBA-CLAIRE was supported by the German Max Planck Society. Figure 2 was produced by the UW-Madison CIMSS GOES Biomass Burning Monitoring Program. Figure 4 was originally produced by Instituto Nacional de Pesquisas Espaciais, Brazil. Special thanks to Robert Chatfield for comments on a draft of this paper. We acknowledge the comments of the anonymous reviewers, which improved the discussions of the presented technique.

References

Albrecht, R., V. Ramanathan, and B. A. Boville, The effects of cumulus moisture transports on the simulation of climate with a general circulation model. *J. Atmos. Sci., 43*, 2443-2462, 1986.

Andreae, et al., Biomass burning emissions and associated haze layers in amazonia, *J. Geophys. Res., 93*, 1509-1527, 1988.

Anthes, R. A., A cumulus parameterization scheme utilizing a one-dimensional cloud model. *Mon. Weather Rev., 105*, 270-286, 1977.

Artaxo P., F. Gerab, M. A. Yamasoe, and J. V. Martins, Fine model aerosol composition in three long-term atmospheric monitoring sampling stations in the Amazon Basin. *J. Geophys. Res., 99*, 22,857-22,867, 1994.

Artaxo P., E. T. Fernandes, J. V. Martins, M. A. Yamasoe, P. V. Hobbs, W. Maenhaut, K. M. Longo, and A. Castanho, Large-scale aerosol source apportionment in Amazonia, *J. Geophys. Res., 103*, 31,837-31,847, 1998.

Chatfield, R. B., and A. C. Delany, Convection links biomass burning to increased tropical ozone: however, models will tend to overpredict O_3, *J. Geophys. Res., 95*, 18,473-18,488, 1990.

Chatfield, R. B., J. A. Vastano, H. B. Singh, and G. Sachse, A general model of how fire emissions and chemistry produce african/oceanic plumes (O_3, CO, PAN, smoke), *J. Geophys. Res., 101*, 24,279-24,306, 1996.

Climanálise: Boletim de monitoramento e análise climática, Instituto Nacional de Pesquisas Espaciais, vol. 13, N. 03, São José dos Campos, São Paulo, Brazil, 1998.

Cohen, J. C., M. A. F. Silva Dias and C. A. Nobre, Environmental conditions associated with Amazonian squall lines: A case study, *Mon. Weather Rev., 123*(11), 3163-3174, 1995.

Crutzen, P. J., and M. Andreae, Biomass burning in the tropics: impact on atmospheric chemistry and biogeochemical cycles, *Science, 250*, 1669-1678, 1990.

Dickerson, R. R., et al., Thunderstorms: An important mechanism in the transport of air pollutants, *Science, 235*, 460-465, 1987.

Emanuel, K.A., and D. J. Raymond, *The Representation of Cumulus Convection in Numerical Models*, Meteorol. Monogr. Ser., 246 pp., Am. Meteorol. Soc., Boston, Mass., 1993.

Fishman, J., J. M. Hoell Jr., R. D. Bendura, V. W. J. H. Kirchhoff, and R. J. McNeal Jr., NASA GTE TRACE-A Experiment (September-October 1992): Overview, *J. Geophys. Res., 101*, 23,865-23,879, 1996.

Fortune, M., and V. E. Kousky, Two severe freezes in Brazil: Precursors and synoptic evolution, *Mon. Weather Rev., 111*, 181-196, 1983.

Freitas, S. R., K. M. Longo, M. A. F. Silva Dias, and P. Artaxo, Numerical modelling of air mass trajectories from the biomass burning areas of the Amazon Basin, *Ann. Acad. Bras. Cienc., 68*, 193-206, 1996.

Fuelberg, H., R. O. Loring, M. V. Watson, M. C. Sinha, K. E. Pickering, A. M. Thompson, G. W. Sachse, D. R. Blake, and M. R. Schoeberl, TRACE-A trajectory intercomparison, 2, Isentropic and kinematics methods, *J. Geophys. Res., 101*, 23,927-23,939, 1996.

Haagenson, P. L., Y.-H. Kuo, and M. Skumanich, Tracer verification of trajectory models, *J. Clim. Appl. Meteorol., 26*, 410-426, 1987.

Kahl, J. D. and P. J. Samson, Uncertainty in trajectory calculations due to low resolution meteorological data, *J. Clim. Appl. Meteorol., 25*, 1816-1831, 1986.

Kalnay, E., et al., The NCEP/NCAR 40-year Reanalysis Project, *Bull. Am. Meteorol. Soc., 77*(3) 437-471, 1996.

Kousky, V. E., and N. J. Ferreira, Interdiurnal surface pressure variations in Brazil: Their spatial distribution, origins and effects, *Mon. Weather Rev., 109*, 1999-2008, 1981.

Kuo, Y.-H., M. Skumanich, P. L. Haagenson, and J. S. Chang, The accuracy of air parcel trajectories as revealed by the observing system simulation experiments, *Mon. Weather Rev., 113*, 1852-1867, 1985.

Longo, K. M.,et al., Correlation between smoke and tropospheric ozone concentration in Cuiabá during Smoke, Clouds, and Radiation-Brazil (SCAR-B), *J. Geophys. Res., 104*, 12,113-12,129, 1999.

Malkus, J. S., C. Ronne, and M. Chaffee, Cloud patterns in Hurricane Daisy, *Tellus, 13*, 8-30, 1961.

Molinari, J., A general form of Kuo's cumulus parameterization, *Mon. Weather Rev., 113*, 1411-1416, 1985.

Petterssen, S., *Weather Analysis and Forecasting*, vol. 1, 428 pp., McGraw-Hill, New York, 1956.

Pickering, K. E., A. M. Thompson, D. P. McNamara, and M. R. Schoeberl, An intercomparison of isentropic trajectories over the South Atlantic, *Mon. Weather Rev., 122*, 864-879, 1994.

Pickering, K. E.,et al., Convective transport of biomass burning emissions over Brazil during TRACE-A, *J. Geophys. Res., 101*, 23,993-24,012, 1996a.

Pickering, et al., TRACE-A trajectory intercomparison, 1, Effects of different input analyses, *J. Geophys. Res., 101*, 23,909-23,925, 1996b.

Pielke, R. A.,et al., A comprehensive meteorological modeling system - RAMS, *Meteorol. Atmos. Phys., 49*, 69-91, 1992.

Satyamurty, P., C. A. Nobre, and P. L. Silva Dias, *Meteorology of the Southern Hemisphere*, vol. 27, edited by D. J. Karoly and D. G. Vincent, pp. 119-139, Am. Meteorol. Soc., 1998.

Seibert, P., Convergence and accuracy of numerical methods for trajectory calculations, *J. Appl. Meteorol., 32*, 558-566, 1993.

Silva Dias, M. A. F., and R. N. Ferreira, Application of a linear spectral model to the study of Amazonian squall lines, *J. Geophys. Res., 97*, 20,405-20,419, 1992.

Simpson, J., and V. Wiggert, Models of precipitating cumulus towers, *Mon. Weather Rev., 97*, 471-489, 1969.

Thompson, A. M., K. E. Pickering, R. R. Dickerson, W. G. Ellis Jr., D. J. Jacob, J. R. Scala, W-K. Tao, D. P. McNamara, and J. Simpson. Convective transport over the central United States and its role in regional CO and ozone budgets, *J. Geophys. Res., 99*, 18,703-18,711, 1994.

Tremback, C. J., Numerical simulation of a mesoscale convective complex: Model development and numerical results, Ph.D. dissertation, 1990, Dep. of Atmos. Sci., Colo. State Univ., Fort Collins.

Tripoli, G. R., and W. R. Cotton, The Colorado State University three-dimensional cloud/mesoscale model - 1982, part I: General theoretical framework and sensitivity experiments, *J. Res. Atmos., 16*, 185-219, 1982.

M. O. Andreae and H. Fischer, Max Planck Institute for Chemistry, Mainz, Germany.

P. Artaxo, Instituto de Física, University of São Paulo, São Paulo, Brazil.

S. R. Freitas and K. M. Longo, NASA Ames Research Center, Moffett Field, CA 94035-1000

M. A. F. Silva Dias and P. L. Silva Dias, Departamento de Ciências Atmosféricas, University of São Paulo, Rua do Matão 1226, 05508-900 São Paulo, Brazil. (mafsdia@-model.iag.usp.br)

(Received October 29, 1999; revised March 23, 2000; accepted March 28, 2000.)